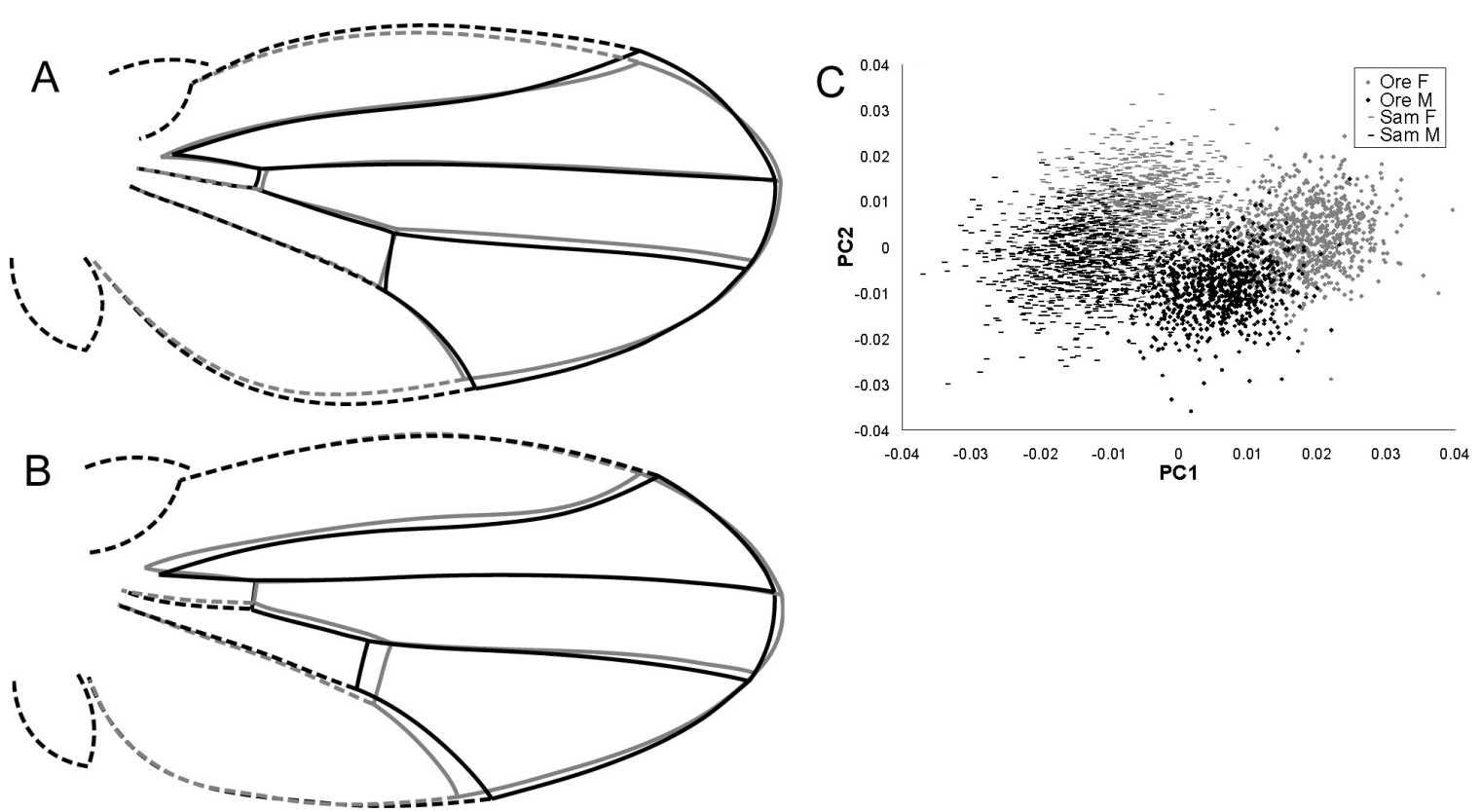
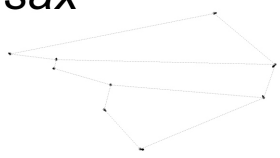


S1. The effects of mutations on wing shape. A) When the mutations are examined in each background separately a similar picture is observed as compared to the combined analysis as shown in Figure 2. In a number of instances, the mutations show a significant effect in one genetic background, but not the other, consistent with strong background effects. B) Including centroid size as a covariate does not alter the strength of the association between mutant genotype and wing shape. This suggests that the effects of the mutations on shape are invariant to allometry with size.



S2. The effect of sex and genetic background on wing shape. A) The effect of sex on wing shape. Males (black) differ subtly from females (grey) largely in a widening of the wing. The majority of the shape difference between the sexes is a consequence of allometry (see text). B) The two genetic backgrounds used for the introgression of mutations demonstrate profound differences in shape. The Sam strain (black) shows a strong proximal shift for the posterior cross vein relative to the Ore-R strain (grey). In addition, there is a relative distal displacement of Sam relative to Ore-R in the posterior region of the wing. The magnitude of the vectors were multiplied by 3X to facilitate visual inspection. Solid segments represent estimated connections between landmarks sampled in this study. The dashed lines are used to illustrate the remaining wing morphology. C) Separation of genetic background and sex effects by principal components analysis. The first and second principal components from the entire data set clearly represent the variation due to background and sex respectively. Within each background and sex combination, the mutant genotypes can be found, clearly demonstrating that they provide a much smaller amount of variation for the data set.

sax^{KG07525}



sax⁴



dad^{J1E4}



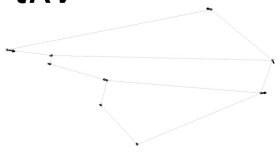
mad^{K00237}



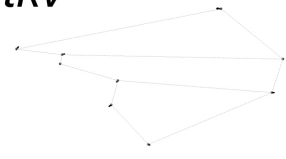
mad^{KG00581}



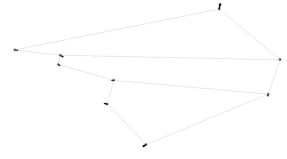
tkv^{K19713}



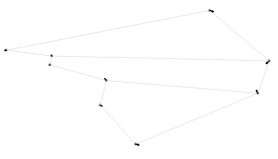
tkv^{KG01923}



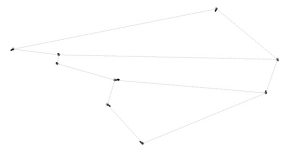
PKA-C-3^{KG00222}



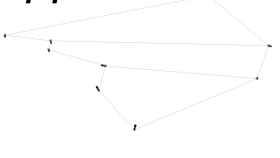
cos^{K16101}



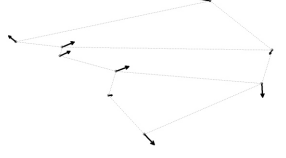
tsh^{A3-2-66}



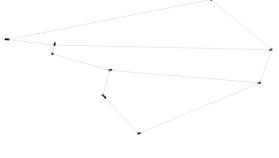
dpp^{KG08191}

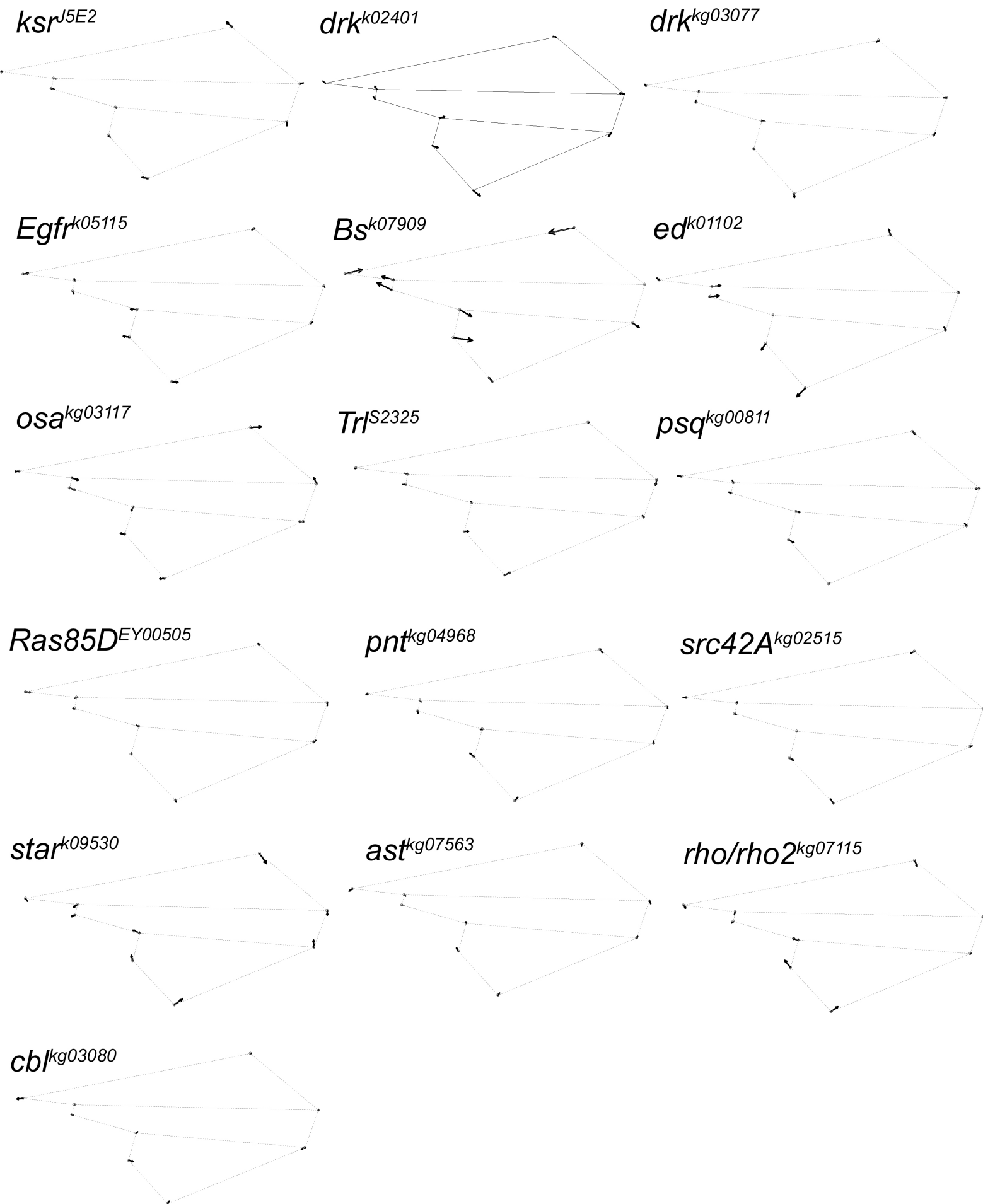


omb^{md653}

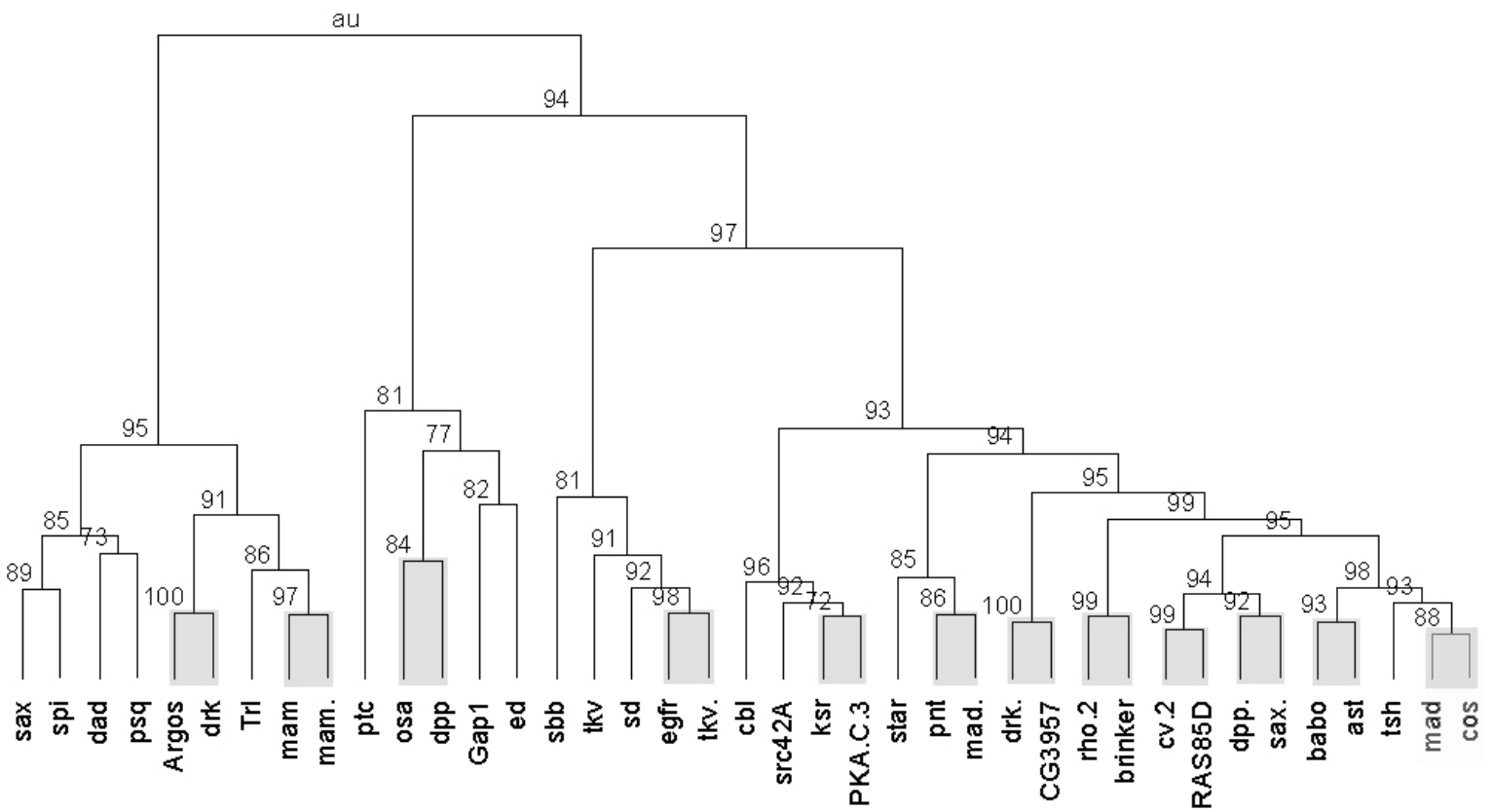


babo^{K16912}

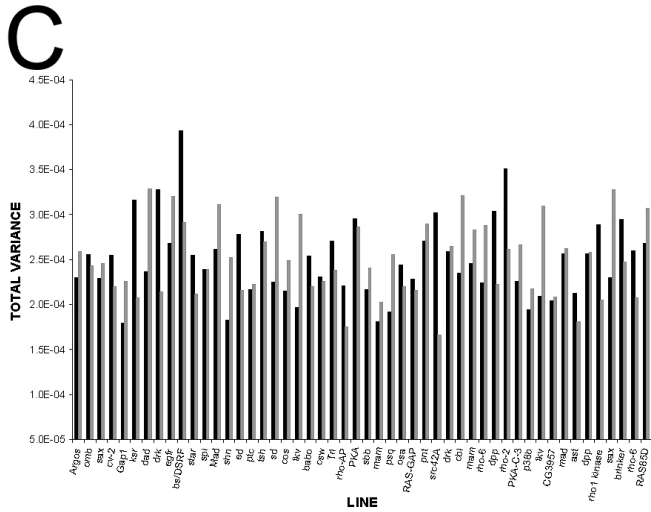
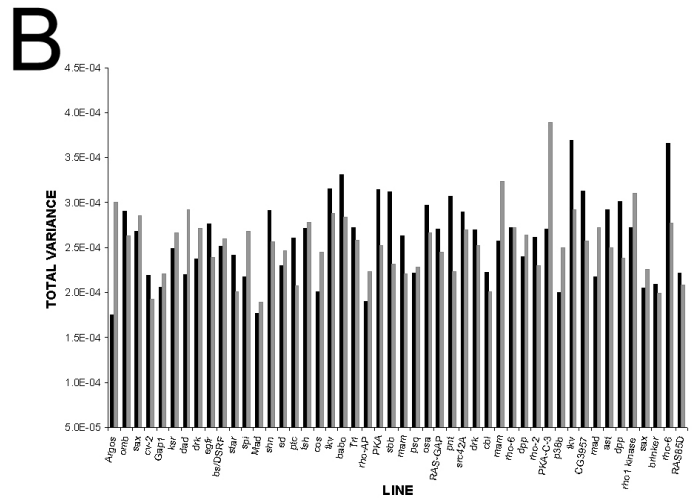
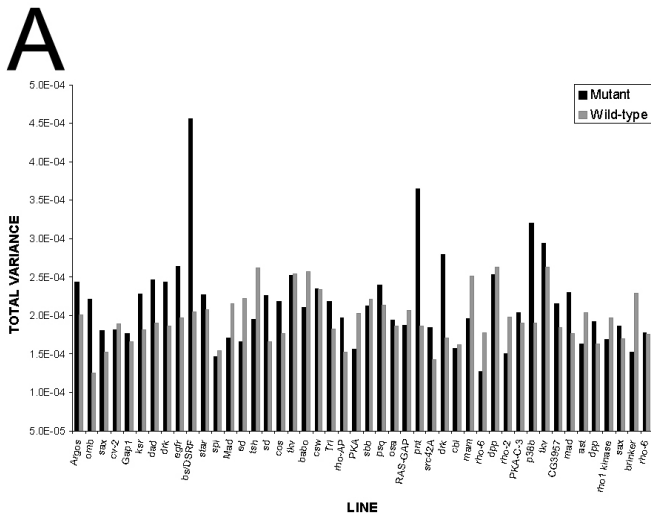




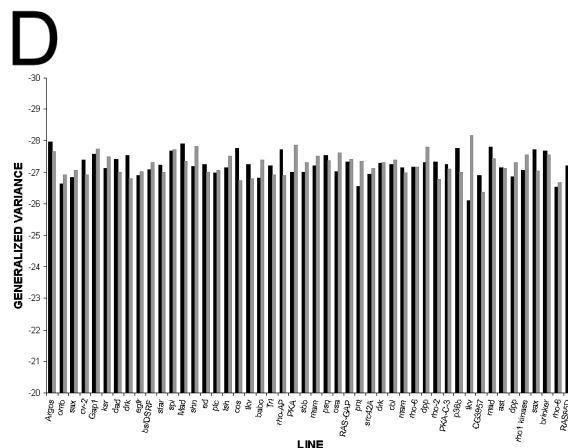
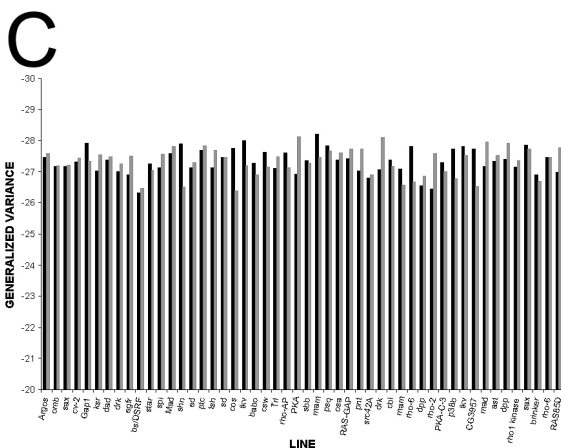
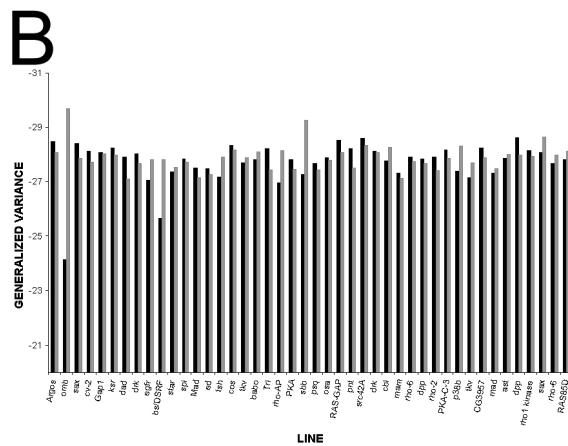
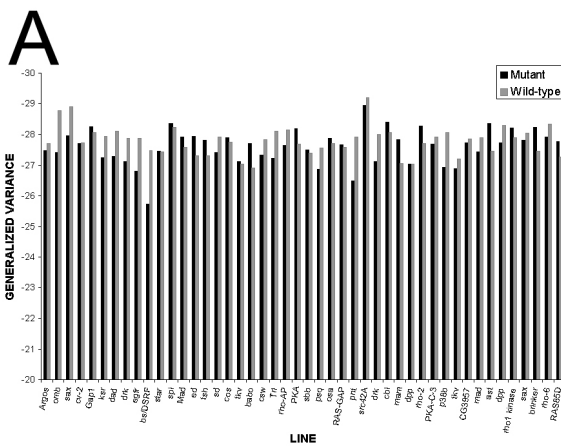
S3. Vector diagrams illustrating the effects of the mutations on wing shape. This included all of the mutations that showed significant effects, but that were not included in Figure 4. This diagram is separated loosely by signal transduction pathways. When there are two mutations in the same gene, they tend not to show similar effects on wing shape.



S4. Phenogram based on hierarchical clustering of wing shape. Numbers at each node represent the approximately unbiased bootstrap value for support for that branch point based on 10000 bootstraps. For this figure, the Euclidean distance metric was used in combination with Ward's algorithm for agglomeration. Highlighted in grey are nodes that were robust to a variety of different distance metrics and agglomeration rules. While there tends to be strong support at the terminal nodes between individual mutations, larger aggregate clusters of mutants tend not to show a high level of support. This picture clearly demonstrates that the mutations are not clustering simply based upon the signalling pathway from which they are canonical members.



S5. The amount of total variance as measured by line, for each genetic background and sex. A) Oregon-R females. B) Samarkand males. C) Samarkand females. While it has been previously predicted that mutant individuals should show higher overall levels of residual variance as compared to their wild-type congenics, this is clearly not a generality. Instead several mutations such as *omb*, *bs* and *pnt* show a large increase, while the majority show virtually no change. There is some evidence for background specific increases in within-line variation.

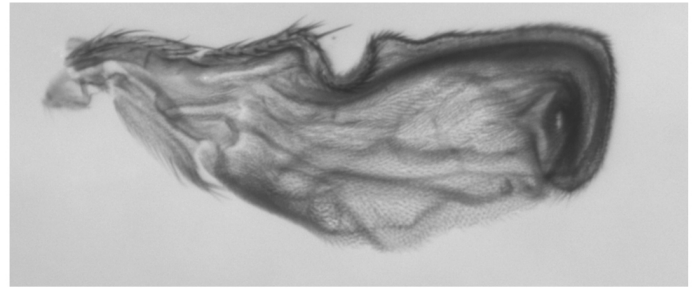


S6. The generalized variance as measured by line, for each genetic background and sex. A) Oregon-R females. B) Oregon-R males. C) Samarkand females. D) Samarkand males. Consistent with the observations for the total variance, there is no evidence for a general trend for the mutants to increase generalized variance relative to their wild-type congenics. This suggests that there is no general change in the pattern of covariation across landmarks.

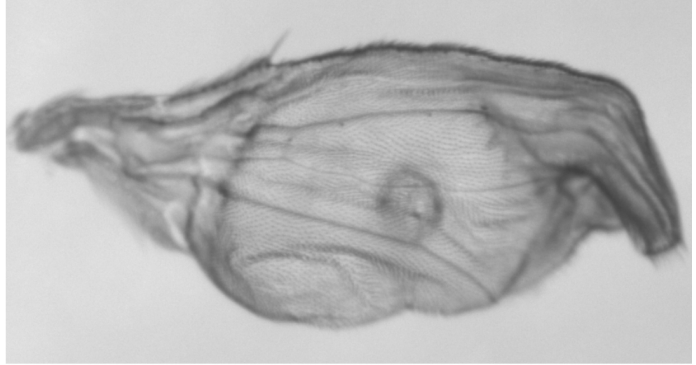
A



B



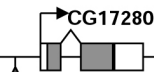
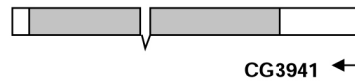
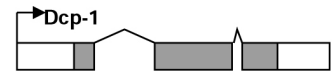
C



D

1000 bp

P element insertion site region ▼



S7. Preliminary analysis of insertion kg07581, a putative mutation in CG3957. The insertion is at 59E3 on the right arm of chromosome 2, located close to the start site to CG3957. The gene ontology for CG3957 predicts that it encodes a transmembrane receptor protein with serine/threonine kinase activity. In the homozygous state, the mutation shows a failure for proper wing expansion consistent with a defect in wing morphogenesis (A). In particular, it appears that the dorsal and ventral layers of the wing do not demonstrate proper lamination, resulting in a variety of phenotypes ranging from a relatively mild convexity in the wing, with regional “wrinkles” where there is local failure in lamination, to strong blistering phenotypes (B), or unexpanded wings (C). This phenotype was observed in both independent introgressions of the kg07581 insertion into two different genetic backgrounds. Based upon this phenotype we have provisionally named the gene *wing morphogenesis defect (wmd)*, for its wing phenotype. Based upon data deposited in the gene expression omnibus, CG3957 appears to be highly expressed in the wing disc. It is worth noting that the insertion is in a region with high gene density (D), thus the insertion may exert its effect on one or more other genes as well.